

Research article

Sujitha Puthukodan, Eljesa Murtezi, Jaroslaw Jacak* and Thomas A. Klar

Localization STED (LocSTED) microscopy with 15 nm resolution

<https://doi.org/10.1515/nanoph-2019-0398>

Received October 1, 2019; revised January 6, 2020; accepted January 29, 2020

Abstract: We present localization with stimulated emission depletion (LocSTED) microscopy, a combination of STED and single-molecule localization microscopy (SMLM). We use the simplest form of a STED microscope that is cost effective and synchronization free, comprising continuous wave (CW) lasers for both excitation and depletion. By utilizing the reversible blinking of fluorophores, single molecules of Alexa 555 are localized down to ~5 nm. Imaging fluorescently labeled proteins attached to nanoanchors structured by STED lithography shows that LocSTED microscopy can resolve molecules with a resolution of at least 15 nm, substantially improving the classical resolution of a CW STED microscope of about 60 nm. LocSTED microscopy also allows estimating the total number of proteins attached on a single nanoanchor.

Keywords: stimulated emission depletion (STED) microscopy; single-molecule localization microscopy (SMLM); protein nanoanchors; single-molecule imaging.

1 Introduction

For more than a century, the diffraction limit of light was considered to be the major barrier in optical microscopy according to Abbe [1]. This limit was overcome with new

far-field fluorescence microscopy techniques by mainly exploiting transient molecular ON and OFF states [2, 3]. Optical triggering and reversible molecular switching laid the foundation for the development of super-resolution microscopy (SRM), which started with the development of stimulated emission depletion (STED) microscopy [4–6], followed by other techniques such as photoactivated localization microscopy (PALM) [7, 8], stochastic optical reconstruction microscopy (STORM) [9], etc., facilitating nanoscale resolution. The whole field of far-field fluorescence microscopy has been revolutionized since then and, as a result, visualization of details that are smaller than the diffraction limit of light became feasible [10, 11].

In STED microscopy and related techniques, one uses the spatial depletion of molecules such that fluorescence occurs only within a predefined, nanoscopic spatial area. This is achieved by overlapping a regularly focused excitation beam with a red-shifted “STED beam” or “depletion beam” in the shape of a donut with a zero central intensity. The effective excitation to the molecular state S_1 persists only at the donut center, while the molecules on the periphery are depleted through stimulated emission from the S_1 state to the ground state S_0 [4–6]. The very first STED microscope consisted of tightly synchronized trains of laser pulses for both excitation and depletion beams [5, 6]. With a typical resolution of less than 30 nm for organic fluorophores, this is considered a choice for many applications. However, the precise synchronization of pulses, proper maintenance, and expensive instrumentation make the “all-pulsed” STED microscope rather complex. In a further development, this complexity was simplified to a great level by using CW lasers for depletion or also for excitation [12, 13] but at the cost of resolution, which was around 50–60 nm. Implementation of gated STED (g-STED) again helped to sharpen the effective point spread function (PSF), thereby improving the on-off contrast, by selectively adjusting the temporal detection window to the fluorophore lifetime, and a resolution of less than 45 nm was achieved (see the sketches in Figure 1) [14, 15]. Many other variations were also introduced such as T-REX STED [16], RESCue-STED [17], MINFIELD [18], DyMIN [19], etc. They all improved STED performance by

*Corresponding author: Jaroslaw Jacak, University of Applied Sciences Upper Austria, Garnisonstraße 21, 4020 Linz, Austria, e-mail: Jaroslaw.Jacak@fh-linz.at. <https://orcid.org/0000-0002-4989-1276>

Sujitha Puthukodan and Thomas A. Klar: Institute of Applied Physics and Linz Institute of Technology (LIT), Johannes Kepler University, Altenberger Straße 69, 4040 Linz, Austria

Eljesa Murtezi: Institute of Applied Physics and Linz Institute of Technology (LIT), Johannes Kepler University, Altenberger Straße 69, 4040 Linz, Austria; and Department of Polymer Science and Technology, Istanbul Technical University, Maslak 34469, Istanbul, Turkey

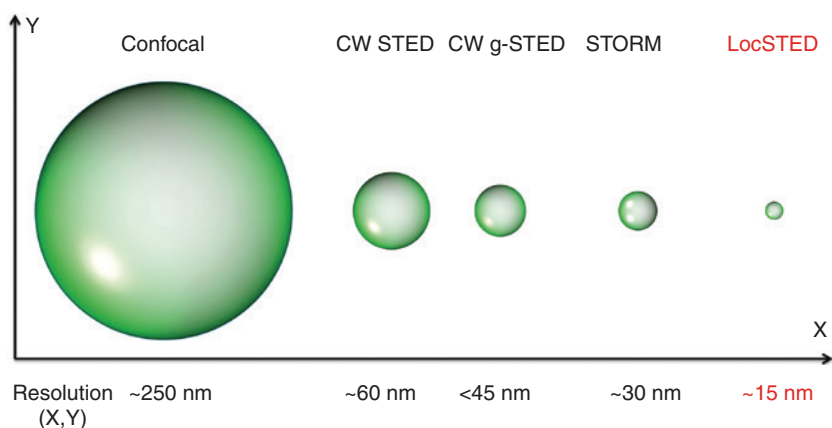


Figure 1: Lateral effective PSFs typically obtained using different microscopy techniques. A comparison of effective PSFs in lateral direction is shown. The PSFs are mutually on scale.

depleting the fluorescence in a more efficient way, i.e. by improving the imaging conditions, utilizing the transitions between molecular states in more controlled ways, maximizing the photon flux, etc., although the complexity of implementation of the respective STED imaging systems increased.

In parallel, wide-field illumination-based SRM techniques, such as PALM and STORM, using stochastic switching or blinking of fluorophores in time and relying on localization and reconstruction of single molecule signals were developed [7–9]. PALM and STORM systems are comparatively simple to implement, but data analysis is more complex and specific fluorophores are required. It was later shown through direct stochastic optical reconstruction microscopy (dSTORM) [20] that conventional fluorophores can also be efficiently used and a resolution of ~30 nm is achievable. In order to improve the photostability and overall localization microscopy performances, different types of imaging buffers, starting from enzymatic oxygen scavenging systems [21, 22] to a reducing and oxidizing system (ROXS) [23–25], were developed. This subsequently improved the control of blinking and significantly reduced photobleaching.

To date, PALM and STORM have achieved a resolution down to 10 nm and a precision approaching 1 nm [26, 27]. Localization better than 10 nm was achieved using pulsed STED and down to 1 nm by MINFLUX where a single donut-shaped laser beam was used to track single molecules [28, 29]. The sizes of the PSFs and resolutions achieved in routine setups can be well estimated by the numbers given in Figure 1.

In this article, we introduce a combination of both STED microscopy and SMLM, i.e. localization with STED (LocSTED) microscopy (Figure 1, right sketch). This combination allows enhancing the spatial resolution and

finding the accurate position of the molecule at the same time. We demonstrate a cost-effective, simple-to-implement, synchronization-free CW STED microscope using diode-pumped solid-state (DPSS) lasers for CW excitation by 532 nm and CW depletion by 660 nm. With LocSTED microscopy, single molecules of Alexa 555 are localized and the molecular coordinates are determined with a localization error of ~5 nm. A resolution of at least 15 nm is obtained. In order to improve the photostability of Alexa 555 fluorophores, an enzymatic oxygen-scavenging system together with a ROXS was developed.

2 Methods

2.1 Experimental

LocSTED imaging was performed on a homemade CW STED microscope using DPSS lasers as shown in Figure S1. Alexa 555 fluorophores were excited using 532 nm CW laser light (Verdi-V5, Coherent, Santa Clara, CA, USA) and depleted using 660 nm CW laser light (Laser Quantum Opus, Germany), and they were imaged with a Leica objective lens (HC PL APO 63X, NA = 1.30 GLYC, Leica Microsystems, Germany). A vortex phase plate (RPC Photonics, Rochester, NY, USA) was placed in the STED beam path in order to obtain a $0-2\pi$ vortex phase pattern. The STED and excitation beams were overlapped and aligned using two dichroic mirrors. The fluorescence signal was collected using a bandpass emission filter (605/70, Chroma Technology Corporation, USA) and detected using a single-photon counting avalanche photodiode detector (APD; Micro Photon Devices s.r.l, Italy). The pixel size for sample-stage scanning was set to 2 nm for LocSTED imaging. The pixel

dwell times varied from 1 to 10 ms for different measurements. Scanning was performed using a three-axis XYZ piezo stage with a travel range of $100 \times 100 \times 100 \text{ }\mu\text{m}$ (P-611.3S Nanocube, Physik Instrumente, Germany) and a position accuracy of 1 nm. The piezo stage was driven by a position controller (E-664 LVPZT position servo controller, Physik Instrumente, Germany). More details on the preparation of samples and imaging buffer are given in Supplementary Information.

2.2 LocSTED data analysis

The images were analyzed using Fiji and MATLAB. A series of images showing individual fluorescence events temporally switched ON and OFF during LocSTED imaging were recorded and then analyzed using a single-molecule localization algorithm custom-written in MATLAB. The final image was reconstructed from a sequence of 100–200 image frames with 50×50 pixels, each pixel with $2 \times 2 \text{ nm}^2$ in size, and typical pixel dwell times from 1 to 10 ms. Typically, each frame contains sparse traces of blinking fluorophores (single lines) along the fast axis. The temporal blinking properties strongly depend on two parameters, namely on the ROXS buffer and the STED laser power. For image reconstruction, the obtained signals are processed in the following way:

Thresholding: The blinking events in each frame are preselected by applying an image threshold. Candidate pixels are by default pixels whose magnitudes are greater than the average brightness of the frame plus 2.5 times its standard deviation. The pixel candidates that are selected are saved and the ones below the threshold intensity are rejected. In every frame, each line with signals above the threshold is then fitted using a 1D Gaussian model.

Fitting: The candidate pixel's local environment, which is determined by a 14×1 pixel window centered at the intensity maximum, is fitted using a sum of two Gaussian functions in the x-direction. All fitted frames are added to each other, thus creating an intensity map of localizations. The 1D Gaussian fitting is a preprocessing tool for generating a smoothened binary mask, which accounts for all pixels above the threshold.

Binary image: The sum image of all fitted 1D Gaussians is transformed into a black and white (binary) image. In this case, all Gaussian-fitted traces are summed up. Although Gaussian fitting is done on the original data, again only the Gaussian-fitted areas with intensities exceeding the

image threshold are selected. The threshold for the transformation is calculated with inter/intra variance of image segments, which is based on Otsu's algorithm [34]. Pixel intensities within an image segment must be close to each other while they must be well separated from different image segments.

Image cleaning: The binary image is subjected to cleaning of single white pixels or single black pixels in a white region using morphological operations such as dilation followed by erosion [35]. The image subsection is performed well and combines the sometimes disrupted regions, which most probably belong to one single emitter detected in various frames, into one connected region describing a single emitter.

Region extraction: The fully connected regions in the binary image are then extracted using a connectivity of eight pixel neighbors. The extracted fully connected regions create a logical mask, which is finally applied to the sum of the experimental frames. This mask cuts out regions from the sum of experimental data that can be considered as candidates for the cumulative signal of a single blinking emitter.

Characterization of the peaks: For each region, the maximum brightness, centroid, and standard deviation are calculated.

3 Results and discussion

3.1 Imaging of nanoanchors

In order to estimate the resolution enhancement and localization precision achievable with LocSTED microscopy, well-defined test systems were chosen. As a first model system, we applied LocSTED microscopy to look at biofunctionalized nanoanchors of 56 nm in diameter, where Alexa 555 molecules were selectively anchored (see Figure 2A). The nanoanchors were written with STED lithography and biofunctionalized using laser-assisted protein adsorption by photobleaching (LAPAP) [30]. The area where the Alexa 555 can be anchored is limited to the surface of the nanoanchors. However, the total number of molecules per nanoanchor cannot be determined with CW STED or STORM alone, because the resolution of either of them is not sufficient. Figure 2B shows an SEM image of a nanoanchor which is 56 nm in diameter and a STED image obtained using CW excitation with 532 nm

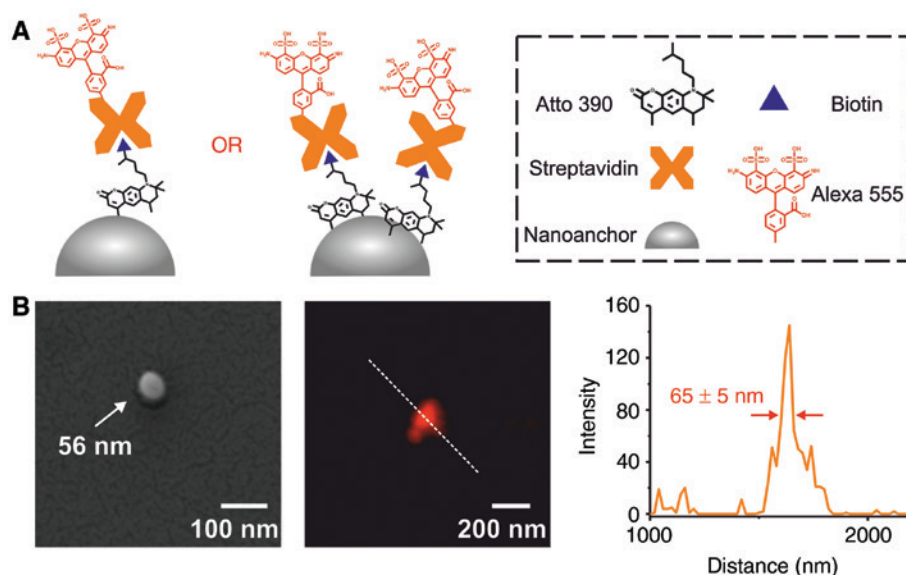


Figure 2: Nanoanchors written using STED lithography and biofunctionalized using LAPAP.

(A) Nanoanchors may carry one or two Alexa 555 tagged Streptavidins, anchored via biotinylated Atto 390 which itself is tagged to the STED-lithographically written nanoanchors via LAPAP. (B) left: SEM image of a nanoanchor with a diameter of 56 nm, center: STED image of a nanoanchor and (right) its corresponding optical FWHM.

(excitation power: 10 μ W) and CW depletion with 660 nm (depletion power: 30 mW). In this case, the corresponding full width at half-maximum (FWHM) of the effective PSF is 65 ± 5 nm.

In LocSTED microscopy, the scanning area is limited to the donut minimum and measures 100×100 nm² (Figure 3A) similar to MINFIELD-STED [18]. All the molecules within the central minimum – no matter whether it is a single molecule or there are multiple molecules that are lying too close to each other – would appear as an ensemble within the resolution limit of the CW STED microscope of ~ 60 nm. We utilize stochastic blinking and localize the single molecules to find their actual positions on the nanoanchors and hence achieve a better resolution. Each nanoanchor is individually focused and scanned with an excitation power of 10 μ W, first with confocal and then with LocSTED, in a subdiffractional region of interest (ROI) measuring 100×100 nm². The pixel size is 2×2 nm² and the pixel dwell time varies from 1 to 10 ms for all measurements. The molecules appeared to be in the ON state stochastically in some of the frames and completely in the OFF states in others. Over the course of time, each molecule undergoes multiple ON/OFF switching cycles. Numerous blinking events across time t are recorded (Figure 3B).

In STED microscopy, the photobleaching comes mainly from the high intensity of the depletion beam. Photobleaching of Alexa 555 was significantly controlled

using ROXS [23–25, 31], which was developed in this case by combining ascorbic acid and methyl viologen together with an enzymatic oxygen scavenging system consisting of glucose oxidase, catalase, and glucose [21]. ROXS helps to depopulate the triplet state, which greatly helps to control the photobleaching and to reduce the photobleaching. The donut is used to deplete the molecule (by stimulated emission and by manipulating the OFF time), and hence the position is estimated within the donut minimum. It was seen that the STED beam, in addition to inducing stimulated emission, was also having an effect on the photobleaching [32, 33] of the molecules, as shown in Figure S2. This improves quenching of the effective fluorescence via the STED beam, in addition to stimulated emission. The power-dependent non-linear behavior of STED with ROXS also shows that the saturation intensity of the fluorophore can be reduced, which means that the STED power required to achieve the desired resolution can be significantly lowered as shown in Figure S3.

The localization of the molecular coordinates from all the image frames, where blinking events appeared, was obtained as described above. All the blinking events are summed up over time t and the final image is reconstructed. The reconstruction of the localized single emitters strongly depends on their stochastic blinking properties and fluorophore bleaching. Figure 4A–C shows the reconstructed images with the sum of

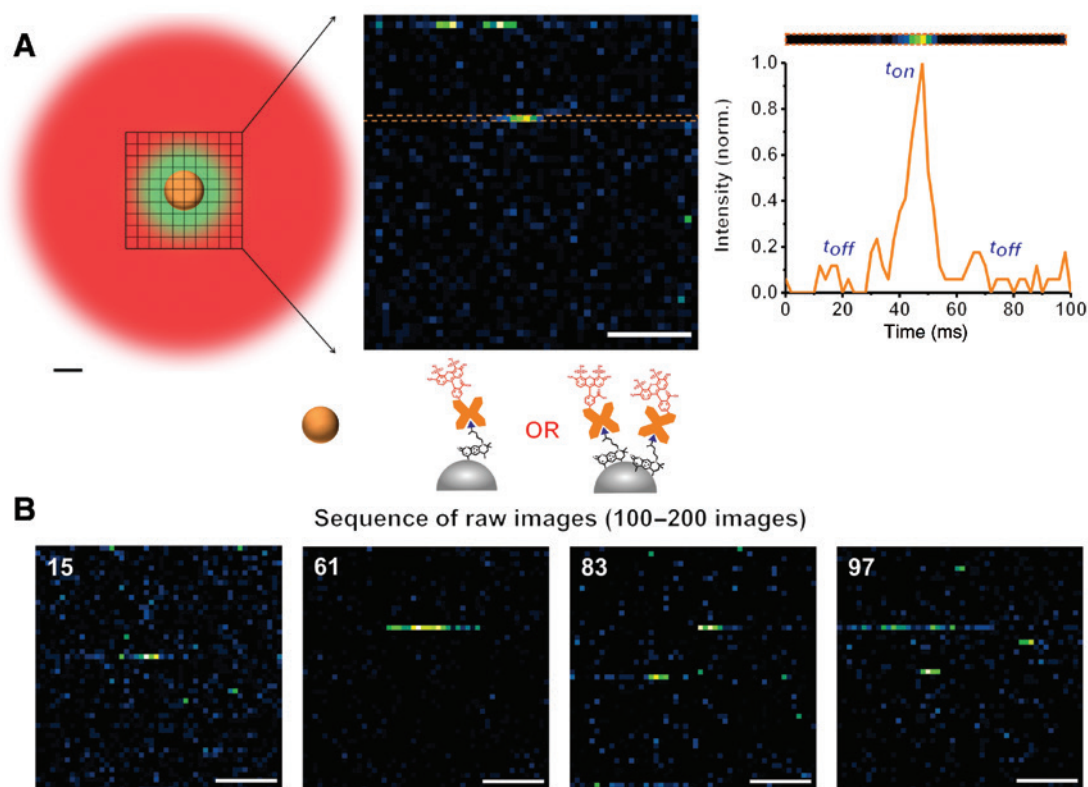


Figure 3: Imaging strategy in LocSTED microscopy.

(A) The scanning field in LocSTED microscopy is limited to a subdiffractional extent. This corresponds to the donut central minimum of $100 \times 100 \text{ nm}^2$ where the depletion beam intensity is moderate. Thus, the molecules are not affected by the maximum of the depletion beam, which further helps to reduce photobleaching. A line scan along a blinking event shows that the ON state typically lasts for $t_{\text{on}} = 10 \text{ ms}$. (B) Examples of frames of raw images that reveal blinking events. Typically, 100–200 images are recorded. All scale bars: 25 nm.

all blinking events (left panels), their Gaussian reconstructions (center panels), and line-cuts through the 2D images (right graphs). The average localization errors are noted above the panels. It was found that, in total, $\sim 56\%$ of the nanoanchors show only one localization event, which can be interpreted that, in most of the cases, only one streptavidin was attached to a nanoanchor (sketch in the right graph). About 39% of the imaged nanoanchors show two localization events, spaced by 16 nm, which hints at two streptavidin per nanoanchor. Three localization events were shown by 5% of the nanoanchors. We note that even in this case, the two Gaussians were easily resolved, and the true resolution was probably much better, close to 10 nm. The fact that we did not observe spacing below 15 nm could be explained by the fact that some minimum distance is required between two streptavidin molecules because of steric hindrance or electrostatic repulsion. This, however, does not exclude the possibility that one streptavidin is doubly labeled with two Alexa 555 molecules, which then, however, would lead to a distance less than 10 nm (see below).

Several more examples are shown in Figure S4. We also carried out simulations by feeding randomly distributed blinking events to the software. In those cases, no artificial clustering was observed by the algorithm (Figure S5). The temporal blinking properties strongly depend on two parameters, namely on the ROXS buffer and the STED laser power.

3.2 Blinking analysis

Once the single molecules are localized, it is also possible to extract the underlying information by having a closer look at the blinking events individually and analyzing the duration of ON-OFF times, their intensity, or their distribution. This will further help to quantify the exact number of fluorophores in a particular localized area. Figure 5A shows a case where a localization event appeared on a nanoanchor, which in a first approximation could be assumed to be a single molecule. In Figure 5B, the total fluorescence intensity is plotted with

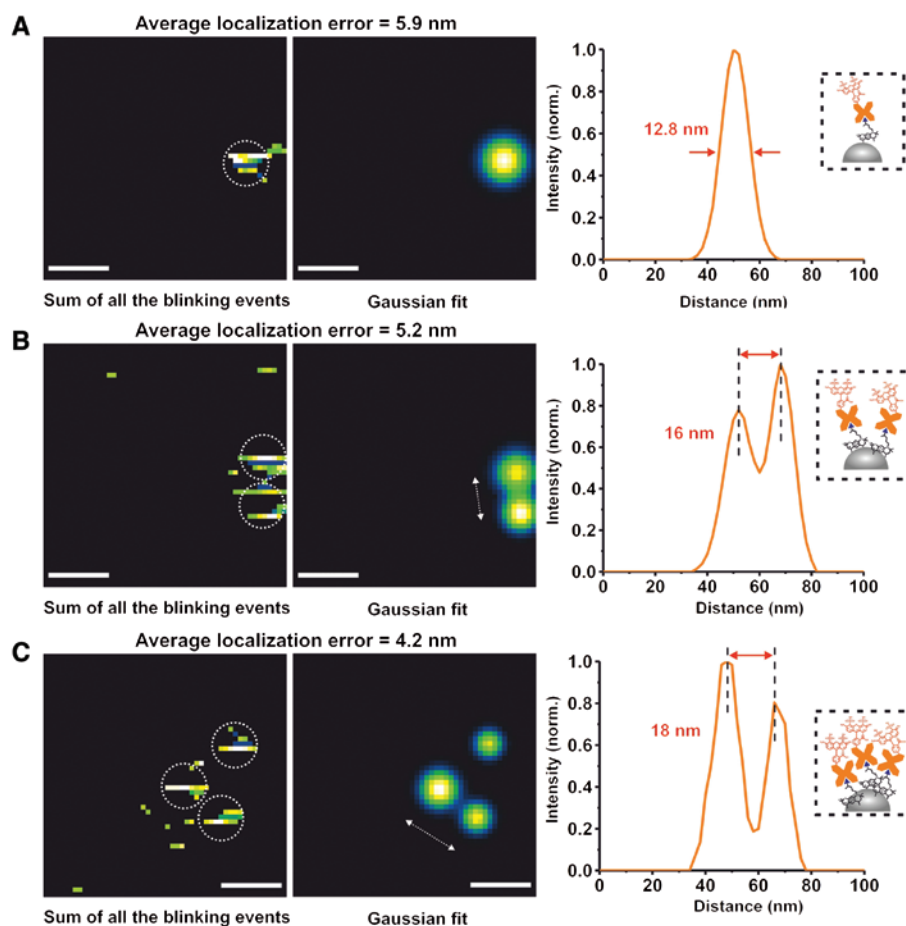


Figure 4: Number of molecules localized on the nanoanchors.

The reconstructed images with the sum of all the blinking events (left panels, the white dashed circles are guides to the eye) and their corresponding Gaussian reconstructions (center panels). The right panels show line scans through the Gaussian reconstructed images. Three different cases are shown: (A) Nanoanchor with a single localization event. The corresponding FWHM of 12.8 nm yields a positioning accuracy of ~ 5 nm. (B) Two localizations with a separation of 16 nm and (C) three localizations, where the lower left two are spaced by 18 nm, indicated by the arrow. All scale bars: 25 nm.

respect to the individual lines from the sum image of all the blinking events. The numbering of the lines is indicated in the left panel of Figure 5A. We take the seventh line as an example since it is the most intense. It actually is twice as intense as other events. It turns out that line 7 appears in frame numbers 61 and 83. In frame 61, the blinking event lasted for ~ 25 ms (orange line in Figure 5C). The event in frame 83 lasted for only 10 ms (blue line) and appeared abruptly while scanning at around 50 ms. The Gaussian reconstruction also shows an unusually broad FWHM of 24 nm (see Figure 5A, right panel). These observations point toward the presence of two fluorophores at the same place, which means a doubly stained streptavidin is observed. Both fluorophores are in the ON state and get recorded at the same time in frame 61. Only

one is in the ON state in frame 83 and it also switches on abruptly during the line scan.

Simulation was also carried out for localized single molecules when the ON probability is changed, as shown in Figure S6. Figure S7 shows the simulation results with simulated blinking events using different spatial orientations and distances.

The localization error is obtained from centroid calculations of each region, which are the candidates for a full signal (the cumulative signal of a single blinking emitter). The blinking rate is adjusted as best as possible via the ROXS buffer to have the blinking emitters very sparsely distributed within individual frames. However, since blinking is a statistical process, it cannot be excluded that a single emitter is turned on and off repeatedly within one line.

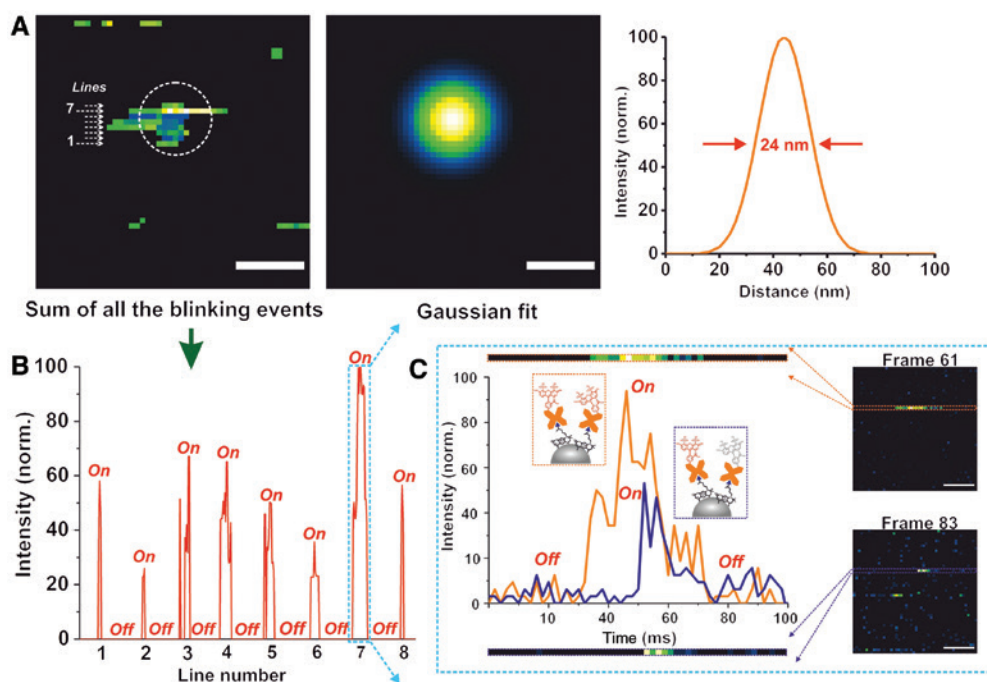


Figure 5: Study of individual blinking events of localized molecules.

(A) Sum of all the blinking events (the white dashed circle is a guide to the eye), their Gaussian reconstruction and the corresponding line profile. (B) Total fluorescence intensity per each line. Line numbers are indicated in the left panel of (A). (C) Total fluorescence intensities plotted in detail for the 7th line, which appears bright in frames 61 and 83. The signal is ON for a longer duration of ~25 ms in frame 61 (orange line) and the total fluorescence intensity is double the intensity compared to that in frame 83 (blue line) which also has a shorter duration of ~10 ms.

Multiple emitters can be rarely observed. Combining multiple times resolved line scans of the same molecule shows a cumulative intensity distribution. Blinking depends also on the intensity of the STED beam, and the ON probability is higher when a fluorophore is in the center of the donut. This increases the resolution. The derived position accuracy for each line would correspond to a temporal fingerprint, but it is not the case if we accumulate all the scans. Figure S8 shows simulated results of the average localization errors obtained in both X- and Y-directions, which are the fast and slow axes, respectively.

3.3 Imaging of DNA origami nanorulers

The second test system we studied was DNA origami nanorulers that carry fluorescent markers on both ends, as shown in Figure 6A. The center-to-center distance between the marks was approximately 50 nm. The DNA origamis carry four biotin molecules and were immobilized on the glass substrate with the help of a BSA-biotin surface incubated with neutravidin solution. Figure 6B

shows the CW-STED image of a DNA origami. Only one unresolved, diffuse feature of ~60 nm FWHM is observed. Figure 6C shows the LocSTED images of a DNA origami where the two dye-tagged ends of the nanoruler are clearly resolved and the distance between them is 50 nm. The sum of all blinking events is displayed in the left panel, and the Gaussian reconstructions are displayed on the right panel.

Figure 7A shows a detailed geometry of a DNA origami. They were fluorescently labeled with Alexa 555 at both ends, and the horizontal center-to-center distance between the two bunches of binding sites for fluorophores was 50 nm. However, the left end actually carries a bunch of eight binding sites spanning an area of 7 nm × 15 nm and the right end carries a bunch of eight binding sites spanning an area of 8 nm × 15 nm, approximately. Hence the expected distance between the two fluorescent spots may vary from slightly less than 50 nm up to approximately 60 nm.

Figure 7B shows a statistical distribution of all the distances that were measured using LocSTED microscopy. Indeed, most of the measured distances are between 50

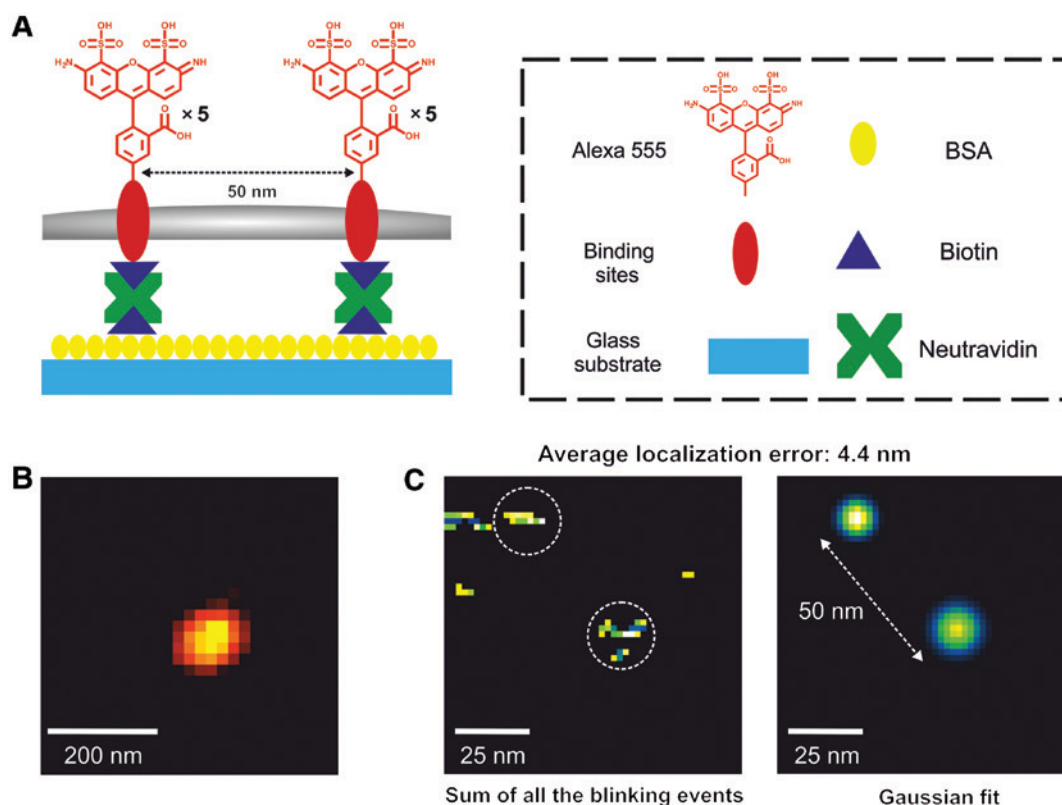


Figure 6: LocSTED microscopy on a DNA origami nanoruler.

(A) Schematic of the DNA origami nanoruler which is immobilized on a BSA-biotin coated surface, incubated with Neutravidin. (B) The CW-STED image of a DNA origami nanoruler shows one blurred image with a FWHM of ~ 60 nm. (C) LocSTED image of a DNA origami nanoruler. Left panel: sum of all the blinking events; right panel: corresponding Gaussian reconstructions. A distance of 50 nm is obtained between the two labeled ends. Note the two different scale bars of 200 and 25 nm in (B) and (C), respectively.

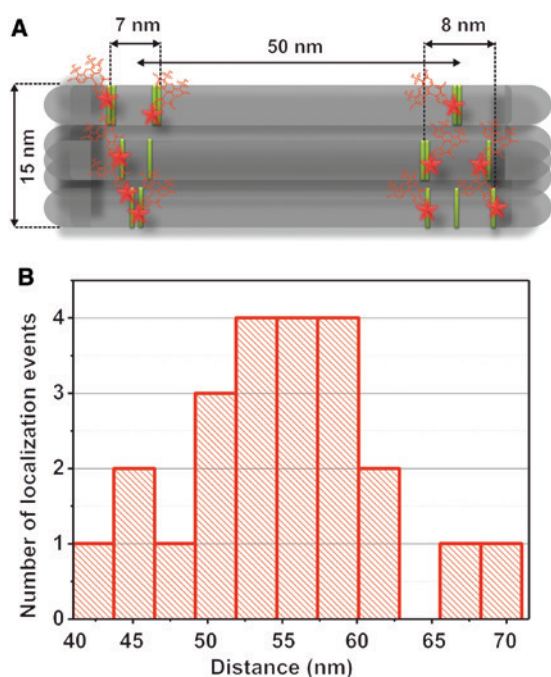


Figure 7: Detailed geometry of a DNA origami nanoruler (A) and a statistical distribution of the distances measured (B).

and 60 nm as expected from the geometry. Distances shorter than 50 nm can be explained by origamis where the innermost binding sites are fluorescently tagged (resulting in spacings down to $50 - 4 - 3.5 = 42.5$ nm) or from an improper horizontal orientation such as tilt or bending of the DNA origamis. Distances above 60 nm could be due to partially unfolded origamis. More examples are shown in Figure S9.

4 Conclusion

In this work, we have combined STED microscopy together with single-molecule localization. This results in LocSTED microscopy, which was implemented by combining the simplest form of STED microscopy comprising CW lasers for excitation and STED. This is not only cost effective but also synchronization-free and easy to implement. The potential of our method was demonstrated by localizing single molecules of Alexa 555, which were attached on nanoanchors written with STED lithography. The closest resolved distance obtained was ~ 15 nm, whereas the

resolution of a classical CW STED microscope is ~ 60 nm. Data analysis was performed using a single-molecule localization algorithm, which was custom-written in MATLAB, and a localization error of ~ 5 nm was obtained. DNA origamis with fluorophores attached on each end and with a center-to-center distance of 50 nm were also used as nanorulers. ROXS as “triplet state controller” proves as a promising choice to suppress the potential photobleaching pathways in STED microscopy, mainly coming from the increased depletion beam intensity. Further, the ROXS buffer renders STED more efficient. Localization better than 10 nm was achieved before using pulsed STED, where nitrogen vacancy defects within diamonds were imaged [28]. However, in LocSTED microscopy, blinking helps to better localize single emitters, although only a CW laser is used for depletion. LocSTED microscopy could also be useful for an enhanced resolution in the axial direction if a bottle-beam STED focus is applied. Applications of SRM techniques are multiplying day by day and, further, LocSTED microscopy can be applied, for example, to study the stoichiometry of membrane proteins in endothelial cells, to have a closer look at clustering of proteins, and so on.

Acknowledgments: We thank Heidi Piglmayer-Brezina, Alfred Nimmervoll, and Bernhard Fragner for technical support. This work was funded by the Austrian Science Fund, Fonds zur Förderung der Wissenschaftlichen Forschung (FWF) (Grant number: W 1250, Funder Id: <http://dx.doi.org/10.13039/501100002428>), under the Doctorate College program “Nano-Analytics of Cellular Systems (NanoCell)”.

References

- [1] Abbe E. Beiträge zur Theorie des Mikroskops und der mikroskopischen Wahrnehmung. *Arch Mikrosk Anat* 1873;9:413–8.
- [2] Hell SW. Microscopy and its focal switch. *Nat Methods* 2009;6:24–32.
- [3] Hell SW. Far-field optical nanoscopy. *Science* 2007;316:1153–8.
- [4] Hell SW, Wichmann J. Breaking the diffraction resolution limit by stimulated emission: stimulated-emission-depletion fluorescence microscopy. *Opt Lett* 1994;19:780–2.
- [5] Klar TA, Hell SW. Subdiffraction resolution in far-field fluorescence microscopy. *Opt Lett* 1999;24:954–6.
- [6] Klar TA, Jakobs S, Dyba M, Egner A, Hell SW. Fluorescence microscopy with diffraction resolution barrier broken by stimulated emission. *Proc Natl Acad Sci U S A* 2000;97:8206–10.
- [7] Betzig E, Patterson GH, Sougrat R, et al. Imaging intracellular fluorescent proteins at nanometer resolution. *Science* 2006;313:1642–5.
- [8] Hess ST, Girirajan TPK, Mason MD. Ultra-high resolution imaging by fluorescence photoactivation localization microscopy. *Biophys J* 2006;91:4258–72.
- [9] Rust MJ, Bates M, Zhuang X. Sub-diffraction-limit imaging by stochastic optical reconstruction microscopy (STORM). *Nat Methods* 2006;3:793–5.
- [10] Hell SW. Toward fluorescence nanoscopy. *Nat Biotechnol* 2003;21:1347–55.
- [11] Hell SW, Sahl SJ, Bates M, et al. The 2015 super-resolution microscopy roadmap. *J Phys D: Appl Phys* 2015;48:443001.
- [12] Willig KI, Harke B, Medda R, Hell SW. STED microscopy with continuous wave beams. *Nat Methods* 2007;4:915–8.
- [13] Moneron G, Medda R, Hein B, Giske A, Westphal V, Hell SW. Fast STED microscopy with continuous wave fiber lasers. *Opt Express* 2010;18:1302–9.
- [14] Vicidomini G, Moneron G, Han KY, et al. Sharper low-power STED nanoscopy by time gating. *Nat Methods* 2011;8:571–3.
- [15] Vicidomini G, Schönle A, Ta H, et al. STED nanoscopy with time-gated detection: theoretical and experimental aspects. *PLoS One* 2013;8:209–15.
- [16] Wildanger D, Medda R, Kastrup L, Hell SW. A compact STED microscope providing 3D nanoscale resolution. *J Microsc* 2009;236:35–43.
- [17] Staudt T, Engler A, Rittweger E, Harke B, Engelhardt J, Hell SW. Far-field optical nanoscopy with reduced number of state transition cycles. *Opt Express* 2011;19:5644–57.
- [18] Göttfert F, Pleiner T, Heine J, et al. Strong signal increase in STED fluorescence microscopy by imaging regions of subdiffraction extent. *Proc Natl Acad Sci U S A* 2017;114:2125–30.
- [19] Heine J, Reuss M, Harke B, D’Este E, Sahl SJ, Hell SW. Adaptive-illumination STED nanoscopy. *Proc Natl Acad Sci USA* 2017;114:9797–802.
- [20] Heilemann M, van de Linde S, Schüttelz M, et al. Subdiffraction-resolution fluorescence imaging with conventional fluorescent probes. *Angew Chem Int Ed Engl* 2008;47:6172–6.
- [21] Yanagida T, Nakase M, Nishiyama K, Oosawa F. Direct observation of motion of single F-actin filaments in the presence of myosin. *Nature* 1984;307:58–60.
- [22] Ha T, Tinnefeld P. Photophysics of fluorescent probes for single-molecule biophysics and super-resolution imaging. *Ann Rev Phys Chem* 2012;63:595–617.
- [23] Nahidiazar L, Agronskaia AV, Broertjes J, van den Broek B, Jalink K. Optimizing imaging conditions for demanding multi-color super resolution localization microscopy. *PLoS One* 2016;11:e0158884.
- [24] Vogelsang J, Kasper R, Steinhauer C, et al. A reducing and oxidizing system minimizes photobleaching and blinking of fluorescent dyes. *Angew Chem Int Ed Engl* 2008;47:5465–9.
- [25] Cordes T, Vogelsang J, Tinnefeld P. On the mechanism of Trolox as antiblinking and antibleaching reagent. *J Am Chem Soc* 2009;131:5018–9.
- [26] Yildiz A, Selvin PR. Fluorescence imaging with one nanometer accuracy: application to molecular motors. *Acc Chem Res* 2005;38:574–82.
- [27] Sauer M, Heilemann M. Single-molecule localization microscopy in eukaryotes. *Chem Rev* 2017;117:7478–509.
- [28] Rittweger E, Han KY, Irvine SE, Eggeling C, Hell SW. STED microscopy reveals crystal colour centres with nanometric resolution. *Nat Photon* 2009;3:144–7.

- [29] Balzarotti F, Eilers Y, Gwosch KC, et al. Nanometer resolution imaging and tracking of fluorescent molecules with minimal photon fluxes. *Science* 2017;355:606–12.
 - [30] Murtezi E, Puthukodan S, Jacak J, Klar TA. Biofunctionalization of sub-diffractionally patterned polymer structures by photobleaching. *ACS Appl Mater Interfaces* 2018;10:31850–4.
 - [31] Kasper R, Harke B, Forthmann C, Tinnefeld P, Hell SW, Sauer M. Single-molecule STED microscopy with photostable organic fluorophores. *Small* 2010;6:1379–84.
 - [32] Eggeling C, Volkmer A, Seidel CAM. Molecular photobleaching kinetics of rhodamine 6G by one and two photon induced confocal fluorescence microscopy. *Chemphyschem* 2005;6:791–804.
 - [33] Ringemann C, Schönl A, Giske A, von Middendorff C, Hell SW, Eggeling C. Enhancing fluorescence brightness: effect of reverse intersystem crossing studied by fluorescence fluctuation spectroscopy. *Chemphyschem*. 2008;9:612–24.
 - [34] Otsu N. A threshold selection method from gray-level histograms. *IEEE Trans Syst Man Cybern B Cybern* 1979;9:62–6.
 - [35] Heijmans HJAM. Morphological image operators. Mishawaka, IN, USA, Academic Press, 1994:25.
-
- Supplementary Material:** The online version of this article offers supplementary material (<https://doi.org/10.1515/nanoph-2019-0398>).